Optical Engineering

OpticalEngineering.SPIEDigitalLibrary.org

Comparison of midwave versus longwave intensity signatures for infrared search and track of small rotorcraft unmanned aerial vehicles

Nicolette Fudala
Robert Short
Jennifer Hewitt
Carl Halford
Teresa Pace
Drew Manville
Mike Theisen
Chris Fearing
Alex Dapore
Craig Olson
Gene Tener
David Gaudiosi
Kathleen Richardson
Ron Driggers

Nicolette Fudala, Robert Short, Jennifer Hewitt, Carl Halford, Teresa Pace, Drew Manville, Mike Theisen, Chris Fearing, Alex Dapore, Craig Olson, Gene Tener, David Gaudiosi, Kathleen Richardson, Ron Driggers, "Comparison of midwave versus longwave intensity signatures for infrared search and track of small rotorcraft unmanned aerial vehicles," *Opt. Eng.* **58**(4), 043107 (2019), doi: 10.1117/1.OE.58.4.043107.

Comparison of midwave versus longwave intensity signatures for infrared search and track of small rotorcraft unmanned aerial vehicles

Nicolette Fudala,[a,*] Robert Short,[a] Jennifer Hewitt,[a] Carl Halford,[b] Teresa Pace,[c] Drew Manville,[c] Mike Theisen,[d] Chris Fearing,[e] Alex Dapore,[c] Craig Olson,[d] Gene Tener,[f] David Gaudiosi,[d] Kathleen Richardson,[a] and Ron Driggers[a]
[a]University of Central Florida, CREOL, The College of Optics and Photonics, Orlando, Florida, United States
[b]University of Memphis, Department of Electrical and Computer Engineering, Memphis, Tennessee, United States
[c]L3 Advanced Laser Systems Technology, Orlando, Florida, United States
[d]L3 Technologies, Inc. Sonoma EO, Santa Rosa, California, United States
[e]L3 Cincinnati Electronics, Mason, Ohio, United States
[f]L3 Space & Sensors, Mason, Ohio, United States

Abstract. Longwave infrared (LWIR) and midwave infrared (MWIR) UAV signature data have been acquired and analyzed in collaboration with L3 Technologies, and we present intensity and root sum square delta T for two rotorcraft unmanned aerial vehicles (UAVs), including the popular DJI Phantom 4 and DJI Inspire, at 0-, 45-, and 90-deg aspect angles. Signature measurements are conducted in the field with clear sky, cloudy, and land backgrounds. We compare MWIR values to that of LWIR for the following criteria: aspect angle, background type, and UAV type. [DOI: 10.1117/1.OE.58.4.043107]

Keywords: infrared; imaging systems; unmanned aerial vehicles; search and track; blackbody signatures; intensity; aspects; outdoor field test; radiometry; measurements.

Paper 190081 received Jan. 20, 2019; accepted for publication Apr. 8, 2019; published online Apr. 30, 2019.

1 Introduction

As small, commercial unmanned aerial vehicles (UAVs) have become an increasing threat toward national, aviation, border, and facility security, the need for infrared search and track (IRST) techniques for these UAV targets has become more important. As general use of UAVs and the availability of smaller, more affordable UAVs increase, so too does the importance of UAV detection and tracking. This is especially a priority for application in security, including airports (as stressed by the U.S. Federal Aviation Administration), borders, prisons, military or defense, national security, and commercial needs. Recent events show that smaller, commercially available UAVs are capable of carrying a payload and carrying out attacks. Earlier in 2018, Venezuelan President Maduro was the target of an attack during a nationally televised military event where 2 DJI M600s, each carrying 1-kg payloads of explosives, were detonated.[1] Other events, such as the Houthi rebels' apparent drone attack on an Abu Dhabi airport in the United Arab Emirates,[2] corroborate the pattern of increasing UAV use in attacks.

While there are many ways to detect UAVs, including radar, LiDAR, acoustics, and machine learning methods, we focus this experiment on passive midwave infrared (MWIR) and longwave infrared (LWIR) optical detection methods.[3–6] Visible range detection methods are less effective, especially in night conditions, while radar technologies have typically been less effective in detecting UAVs of smaller to medium sizes[7,8] since a large part of the vehicle is plastic. Because of IR sensors' ability to detect well both in day and night and their increased detail compared to other methods, MWIR and LWIR optical detection may be a viable method for UAV search, detection, and tacking. The ultimate goal is to validate an IRST model used to develop UAV detection sensors. A source of signatures aids the development of UAV IRST systems. While two papers have explored IR as a sensor method,[6,9] our work extends these prior efforts by providing radiometrically calibrated signature data. Prior to these papers, IRST experiments focused on large-sized UAVs.[7] LWIR signatures are available for one UAV in an indoor, uniform-background setting at different aspects.[9] We present an open source of typical UAV signatures in the field, representative of what would be expected in actual detection conditions. The main purpose of this experiment was to obtain up-close, calibrated radiometric MWIR and LWIR signatures for two commercial UAVs. Signatures were taken at different UAV aspects and in clear sky, cloudy, and terrestrial backgrounds.

2 Data Collection and Analysis Method

In this experiment, intensity data of each UAV and the surrounding backgrounds were collected for LWIR and MWIR. This was later converted into absolute intensity, with root sum square delta T (RSSΔT) and differential intensity to characterize the UAVs in each of the clear sky, cloudy sky, and land backgrounds. Radiometric calibration and formulas as well as target intensity measurements are detailed as follows.

With the automatic gain control disabled on detectors, blackbodies are held at controlled temperatures to facilitate nonuniformity correction (NUC). This is performed by filling the detector's field of view with an object of constant temperature and measuring the spatial noise detected. Following adequate NUC, the system intensity transfer

*Address all correspondence to Nicolette Fudala, E-mail: nicolette.fudala@knights.ucf.edu

function (SITF) is obtained to find the relation between temperature and digital counts on the detector.

Upon completion of blackbody calibrations, analysis of target images is conducted. The SITF is used to estimate the target's apparent temperature, treating each detector area projected onto the target as the equivalent of a Lambertian blackbody. After completing this equivalent blackbody temperature image, the data are then converted into an exitance image with the use of a blackbody emittance function. This is then converted into a radiance image. By incorporating the area on the target that is covered by each pixel into this radiance image, we have the intensity of the image for each pixel:

$$\mathrm{IntImage}(x,y) = \mathrm{PixArea} \times \mathrm{RadImage}(x,y)\ (\mathrm{W/sr}). \quad (1)$$

In which $\mathrm{IntImage}(x,y)$ and $\mathrm{RadImage}(x,y)$ are the intensity and radiance at each pixel (x,y). The total intensity of the target [Eq. (2)] is attained by taking the sum of the intensity at each pixel that pertains to the target itself

$$I_{\mathrm{tgt}} = \sum_{\substack{x=\mathrm{alltgtpix} \\ y=\mathrm{alltgtpix}}} \mathrm{IntImage}(x,y)\ (\mathrm{W/sr}). \quad (2)$$

The most significant quantities to calculate include absolute intensity, differential intensity, and RSSΔT. To determine the absolute intensity, the equivalent blackbody temperature $T(x,y)$ is estimated from the SITF of the radiometer for each pixel. This is integrated over the wavelength range to yield the radiance in $\mathrm{W/cm^2\ sr}$. After multiplying by the area of a pixel in $\mathrm{cm^2}$, where R is the target range and α is the instantaneous field of view, and summing over all target pixels, we have the absolute intensity in W/sr.[10] Absolute intensity [Eq. (3)], in W/sr, is necessary to insert into various scenarios for the design of detection algorithms and systems:[10]

$$I_{\mathrm{tgt}} = \sum_{\substack{x=\mathrm{alltgtpix} \\ y=\mathrm{alltgtpix}}} \frac{1}{\pi}\left(\frac{\alpha R}{10}\right)^2 \int_{\lambda_1}^{\lambda_2} \frac{c_1}{\lambda^5\left\{e^{\left[\frac{c_2}{\lambda T(x,y)}\right]}-1\right\}}\mathrm{d}\lambda\ (\mathrm{W/sr}). \quad (3)$$

Here c_1 is 37418.44 $\mathrm{W/cm^2\ \mu m^4}$ and c_2 is 1.439 cm K.[11] Differential intensity I_D is calculated by taking the difference in the absolute intensity of the target and that of the surrounding background multiplied by the ratio of the number of target pixels p_{tgt} to background pixels p_{bg}. Differential intensity [Eq. (4)], also in W/sr, is used to determine if models are behaving correctly:

$$I_D = I_{\mathrm{tgt}} - I_{\mathrm{bg}}\frac{p_{\mathrm{tgt}}}{p_{\mathrm{bg}}}\ (\mathrm{W/sr}). \quad (4)$$

RSSΔT [Eq. (5)], in units of K, are calculated by subtracting the square of the standard deviation of the target temperature σ_{tgt} from the square of the difference in target and background temperatures and taking the square root.[11] Again, the equivalent blackbody temperature of the target and background, $T(x,y)_{\mathrm{tgt}}$ and $T(x,y)_{\mathrm{bg}}$, is estimated from the SITF of the radiometer for each pixel:

$$\mathrm{RSS}\Delta T = \sqrt{[T(x,y)_{\mathrm{tgt}} - T(x,y)_{\mathrm{bg}}]^2 - {\sigma_{\mathrm{tgt}}}^2}\ (\mathrm{K}). \quad (5)$$

RSSΔT is commonly used in models for assessing the probability of identification by human observers and algorithms.

3 Field Collection

Sensors were stationed at a camp near the SE corner of Shelby Farms in Memphis, Tennessee.[12] A tent housing the cameras was placed at the center of base camp, with surrounding supporting equipment and computers. The north side of the camera tent was left unobscured in order to fly UAVs and capture signatures. UAVs were flown north of the camp over a field and faced south toward base camp. Blackbodies were located close to the camp in the NE direction but still in the FOV of the cameras.

The two rotorcraft UAVs below (Figs. 1 and 2) were used as targets for up-close signatures. Both models are small, commonly available, and relatively inexpensive, making them ideal candidates for potential use as threats. Tests were planned accordingly so that battery usage was manageable with extra batteries. All UAVs were equipped with a standard GPS log system.

- UAV#1: DJI Phantom 4 Pro (350-mm diagonal).
- UAV#2: DJI Inspire 1 (600-mm diagonal).

The following cameras/sensors were used for radiometric measurements. The Viento-G LWIR and HD ORCA MWIR cameras served as the primary sensors for the experiments.

- RAD#1: Viento-G HD LWIR WFOV 16.7-mm lens uncooled microbolometer.
- RAD#2: HD ORCA MWIR WFOV camera.

Table 1 shows resolved–unresolved (1-pixel target size) transition ranges and 50-pixel target size transition ranges for the primary sensors. Targets were placed at much shorter distances from the cameras—between 2 and 3 m—to be sure they are resolved targets with high detail.

Fig. 1 The DJI Phantom 4 Pro, a popular rotorcraft UAV, is shown here as UAV 1.[13]

Fig. 2 The DJI Inspire is shown here as UAV 2.[14]

Table 1 Transition points from resolved to unresolved at 1 and 50 px for each radiometer.

UAV	1 px transition point—ORCA MWIR (m)	50 px transition point—ORCA MWIR (m)	1 px transition point—Viento-G LWIR (m)	50 px transition point—Viento-G LWIR (m)
#1	700	14.00	263.53	5.27
#2	1200	24.00	451.76	9.03

The following blackbodies and equipment were used to calibrate sensors and radiometers. The second 4-paneled blackbody was used under the condition of noninterference, meaning it would operate alongside primary equipment only if doing so would not cause any delay in taking data.

- BB#1: Temperature-adjustable blackbody.
- BB#2: Four-panel blackbody (noninterference).

The experiment, which was the first of a series of three related experiments (to be published), involved obtaining the signatures of each UAV while hovering in a stationary position at different aspect angles and different backgrounds. Aspect angles were 0 deg (front view, shown in Figs. 1 and 2), 4 deg, and 90 deg (side view). Backgrounds included clear sky, cloudy sky, and land. The cameras were located at base camp pointing N-NE. They remained oriented with an upward line of sight for clear sky and cloudy backgrounds, whereas they remained oriented straight forward for land backgrounds. Blackbody locations were to the N-NE, near base camp, and their orientations remained straight toward the cameras. First, calibration images were taken, followed by a series of nine short video clips of UAV 1 hovering at each aspect angle (starting from 0 deg), for each background. This was repeated for UAV 2. The data were collected in morning light conditions with average temperatures around 87°F, humidity levels at 58%, and wind speeds at 0 mph.

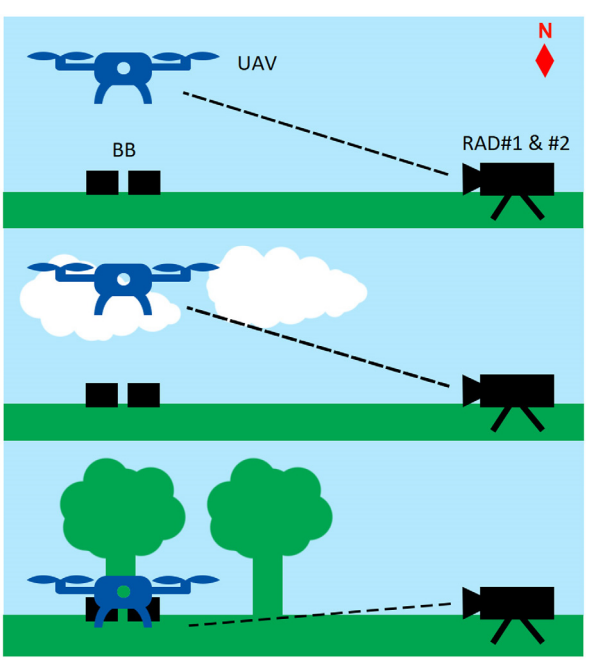

Fig. 3 Side view of setup for clear sky, cloudy, and land backgrounds.

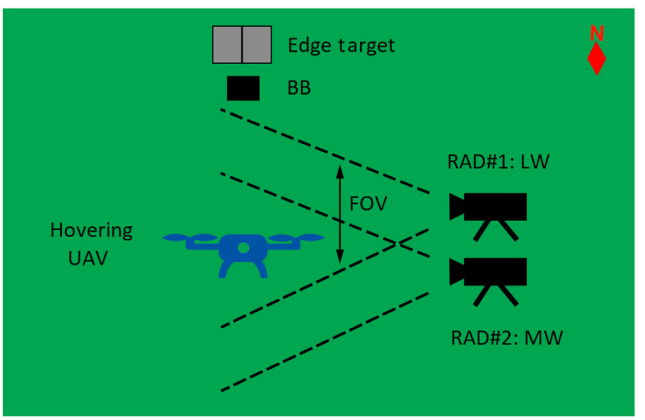

Fig. 4 Top view of Test 1 setup.

Figures 3 and 4 illustrate the arrangement of the equipment for the experiment.

Data collected include calibration images at 20°C and 40°C prior to UAVs, signature images for each UAV at each aspect angle for cloudy and land backgrounds, weather data (including temperature and humidity), and sensor characteristics and settings. Equivalent blackbody temperatures, absolute and differential intensities, and RSSΔT were calculated after processing the files with a MATLAB program for radiometric and sensor calculations called RASGUI that is currently pending publication.[10]

4 Radiometric Calibration and Analysis

Calibrated signatures are obtained using the temperature and intensity calculations described above. Calibration of the signatures yields temperature and intensity values within 5% of the actual temperature.[10] For calibration, both blackbodies were placed on a table ~10 m from the LWIR and MWIR cameras. An edge target was also placed ~5 m to the right of the blackbodies for some calibration images. Before Test 1 for clear sky and land backgrounds, two calibration images were taken. The adjustable blackbody was set to 20°C for one image and 40°C for the second. The four-panel blackbody had static temperatures at 58.4°C, 37.2°C, 32.6°C, and 29.7°C, although it should be noted that this piece of equipment was operated under conditions of noninterference. It should also be noted that the maximum temperature of some signatures yielded calculations outside of the calibration range.

5 Results

Absolute intensity, differential intensity, and RSSΔT are calculated from signatures, camera properties, UAV dimensions, and range. All aspect angles are measured relative to the UAV's orientation when the front of the UAV is directly

facing the camera. The LWIR camera has a spectral range of 8 to 14 μm, with a pixel pitch of 17 μm, and focal length of 12.8 cm. The horizontal field of view (HFOV) and vertical field of view (VFOV) are 48.7 deg and 36.5 deg. The MWIR camera wavelengths range from 3 to 5 μm with a pixel pitch of 8 μm and focal length of 16 cm. The MWIR HFOV and VFOV are 36.7 deg and 20.6 deg. Though it is likely much <1, the emissivity is not assumed because the radiometry is reported in terms of the equivalent flux provided by a blackbody source at a temperature that matches the target emission power.

5.1 *UAV 1: DJI Phantom Pro 4*

The length of the DJI Phantom Pro 4 on its diagonal is 35 cm. Because the UAV is nearly symmetrical, each side of the UAV is ~24.7 cm long. The resolution of the LWIR camera is 2.5863 px/cm and the resolution for the MWIR camera is 5.6170 px/cm. We estimate the range for the LWIR and MWIR cameras are 2.9110 and 3.5600 m, respectively. With these data, we obtained the results shown in Tables 2 and 3.

Table 2 LWIR intensities and RSSΔT for each background and aspect angle with UAV 1.

UAV 1: longwave data				
Background	Aspect angle (deg)	Absolute intensity (W/sr)	Differential intensity (W/sr)	RSSΔT (K)
Clear sky	0	1.4194	0.2301	10.9457
	45	1.4254	0.2147	9.8979
	90	1.6649	0.2490	9.8071
Cloudy	0	1.1521	0.1371	7.9611
	45	1.3395	0.1644	8.0802
	90	1.2867	0.1733	9.0222
Land	0	1.4129	−0.0735	3.2921
	45	1.5465	−0.0633	2.6872
	90	1.7416	−0.0424	1.5897

Table 3 MWIR intensities and RSSΔT for each background and aspect angle with UAV 1.

UAV 1: midwave data				
Background	Aspect angle (deg)	Absolute intensity (W/sr)	Differential intensity (W/sr)	RSSΔT (K)
Clear sky	0	0.0415	0.0101	7.4715
	45	0.0420	0.0120	8.9864
	90	0.0478	0.0130	8.1274
Cloudy	0	0.0329	0.0059	5.4359
	45	0.0350	0.0057	4.8416
	90	0.0370	0.0059	4.7222
Land	0	0.0418	−0.0057	3.6467
	45	0.0445	−0.0051	3.0939
	90	0.0438	−0.0044	2.6639

Outlines were traced by hand, as depicted in Figs. 5 and 6. The MWIR camera, which had better resolution, yielded more detailed features than the LWIR camera, as expected. LWIR intensities were generally greater than those of MWIR. It should be noted that MWIR and LWIR signatures for UAV 1 against the land background were taken after the UAV had been sitting in the sun.

UAV 1 was still detectable and recognizable as the aspect angle changed, generally maintaining the same shape. Clear sky backgrounds provided the most contrast and were easiest to trace, whereas cloudy backgrounds were more difficult as a result of lower contrast. Land background produced some clutter that blended with the UAV in places, but the form of the UAV was still visible.

5.2 *UAV 2: DJI Inspire*

Assuming the front is the longest, the dimensions of the DJI Inspire are 30, 44, and 45 cm in height, width, and length, respectively. Therefore, the resolution of the LWIR camera is 2.2227 px/cm and the resolution of the MWIR camera is 5.3778 px/cm. We estimate the range for the LWIR and MWIR cameras are 3.5820 and 3.8425 m, respectively. With these data, we obtained the results shown in Tables 4 and 5.

UAV 2 has a shape that is distinct in comparison to most rotorcraft UAVs. It is not symmetrical and has a unique mechanism that allows its landing gear to move up and down, resulting in two modes of flight, as shown by the outlines in Figs. 7 and 8.

In general, the LWIR camera provided greater contrast than the MWIR camera. Unlike for UAV 1, the shape and features of UAV 2 changed significantly as aspect angle increased, although it remained recognizable. Clear sky backgrounds provided the most contrast, as was observed for UAV 1. However, cloudy backgrounds only showed slightly lower contrast. Land backgrounds produced more clutter, but the overall temperature of the UAV was different enough from the background to remain easily visible.

5.3 *Charts and Comparisons*

Figures 9–11 quantify all the above data on two graphs—one for absolute intensity and one for RSSΔT—so trends from the different cases can be compared more easily. Each graph is divided into three charts by background: clear sky, cloudy sky, and land. MWIR values are depicted on the left half of each chart, whereas LWIR values are depicted on the right half of each chart. For each MWIR-half and LWIR-half, UAV 1 is represented by a set of bars on the left and UAV 2 is represented by a set of bars on the right. 0-deg, 45-deg, and 90-deg aspects are colored in blue, red, and grey, respectively.

The bar chart below directly compares LWIR to MWIR RSSΔT values for each background and aspect case for UAV 1. "CS," "CL," and "LN" refer to clear sky, cloudy sky, and land backgrounds, respectively, while 0, 45, and 90 refers to the aspect angle in degrees.

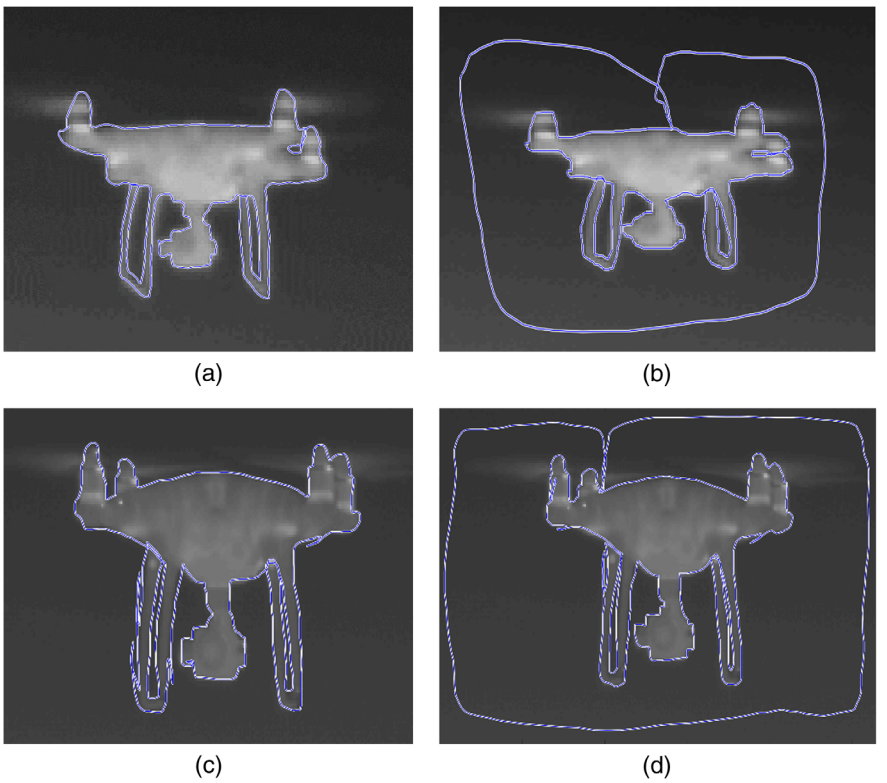

Fig. 5 (a) and (c) Target and (b) and (d) background outlines of (a) and (b) UAV 1 LWIR and (c) and (d) MWIR signatures at 0-deg aspect angle in clear sky.

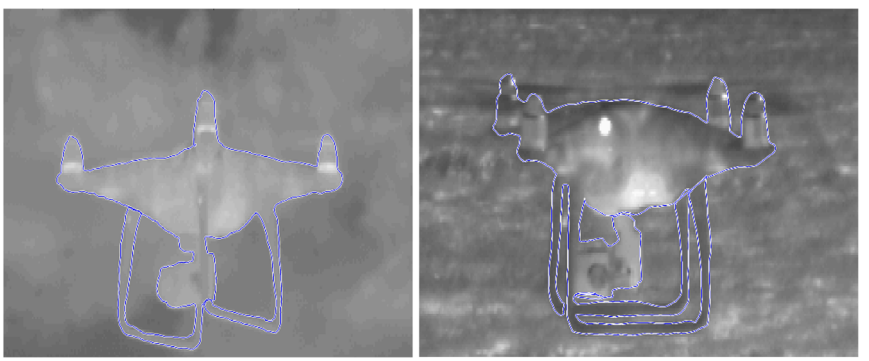

Fig. 6 UAV 1 MWIR signatures at 45- and 90-deg aspect angles in cloudy and land backgrounds, respectively.

6 Blade and Outline Issues

As seen in the images above, the blades of both UAVs were noticeable in MWIR and LWIR. In the results above, the blades were originally omitted from the target outline and included in the background outline because the blade outline was not clearly defined. However, the intensity of the areas where each blade was found consisted of a heterogeneous mixture of background and blade. It was not clear whether the blades should be included as part of the target outline (with an infill 100% or less), background outline, or omitted from both. This highlighted the possibility of error introduced into the results, so the matter was investigated by recalculating the intensities and RSSΔT for each case and determining the percent difference from the original results. The calculation exercise was repeated for MWIR and LWIR with both UAVs at a 0-deg aspect angle in clear sky, which allowed for the best contrast between blade and background.

The three cases are defined as follows:

- Target "with blades" (notated "Tgt w/B") includes the fullest extent of each blade intensity in the target outline and omits it completely from the background outline. The "fullest extent" of the blade is defined as all areas of the blade where the intensity is visibly greater than that of its surrounding background (with minimal processing), assuming an infill of 100% regardless of the level of contrast.
- "Target without blades" (notated "Tgt w/o") omits the blade entirely from the target outline and

Table 4 LWIR intensities and RSSΔT for each background and aspect angle with UAV 2.

UAV 2: longwave data				
Background	Aspect angle (deg)	Absolute intensity (W/sr)	Differential intensity (W/sr)	RSSΔT (K)
Clear sky	0	2.4369	0.3091	8.5825
	45	3.7364	0.5365	9.7425
	90	4.4458	0.6799	10.3422
Cloudy	0	4.1402	0.7315	12.5230
	45	6.5799	1.1971	13.0321
	90	7.1192	1.3063	13.2876
Land	0	2.5830	–0.1401	3.4178
	45	4.4740	–0.2287	3.2218
	90	5.3384	–0.2121	2.5209

Table 5 MWIR intensities and RSSΔT for each background and aspect angle with UAV 2.

UAV 2: midwave data				
Background	Aspect angle (deg)	Absolute intensity (W/sr)	Differential intensity (W/sr)	RSSΔT (K)
Clear sky	0	0.0828	0.0215	8.0899
	45	0.0922	0.0261	8.8932
	90	0.1864	0.0765	14.1907
Cloudy	0	0.1346	0.0560	15.3775
	45	0.2160	0.0821	13.7231
	90	0.2704	0.1126	15.4662
Land	0	0.0876	–0.0181	5.4775
	45	0.1488	–0.0238	4.2706
	90	0.1509	–0.0332	5.8315

includes the fullest extent of each blade in the background outline.

- "Total" without blades (notated "Tot w/o") omits the fullest extent of each blade from both the target and background outlines.

Here the percent difference compares each case below to the original results above. The percent error compares the "target with blades" and "target without blades" values to the "total without blades" value. It should be noted that the background absolute intensity was corrected for the number of target pixels.

The results of the analysis (Table 6) yield errors <6% in all cases for differential intensity, whereas RSSΔT error ranges from 1% to 27%. Intensity difference percentages are below 10% for all UAV 2 cases and UAV 1 case in the MWIR and are below 2% for UAV 1 case in the LWIR. RSSΔT percent differences are up to 30% for target with blade cases but remain below 2% for all others. Although some difference percentages are significantly higher, these values are relative to one another. With that in mind, we can conclude that any approach yields relatively similar results. The error percentages are more telling with respect to the blades' impact overall. We conclude that the error associated with the blade intensity is not significant with respect to differential intensity and therefore negligible. RSSΔT errors are not significant for the "target without blades" case but are significant for the "target with blades" case.

We conclude that the largest errors, mainly seen for the "target with blades" cases, are primarily the result of the increase in area caused by the addition of the background mix and not a result of an increase in intensity. The ratio of the number of pixels with blades to pixels without blades yielded an increase in area by roughly 20%; therefore, 20% of the intensity error is from area increase and not from an increase in flux.

It should be noted that the variation in flux provided by the rotating blades could provide a detection signature if the infrared systems had a short enough integration time and frame rate to exploit the temporal emission signal. Currently, advanced infrared systems that are LWIR VOx and MWIR InSb do not have short enough integration times or time constants to exploit this signal.

The impact of outlining by hand was also investigated by determining the absolute intensity, differential intensity, and RSSΔT percent differences from five trials of outlines around the same image. We chose an LWIR image of UAV 1 in a cloudy background at a 90-deg aspect angle because the image possessed target edges that were less distinct than others. Thus it was more likely to be representative of the possible extent of the outline error. The average percent difference for absolute intensity, differential intensity, and RSSΔT were 1.7610%, 0.6910%, and 1.2848%, respectively. Thus we conclude that the error resulting from outlining the targets by hand was not a significant source of error.

7 Discussion

Generally, MWIR produces more detail than LWIR, likely due to the intrinsically wavelength-limited, lower resolution of the LWIR camera, and significantly more reflections. Results appeared to show hotter temperatures with increased UAV operation and/or sun exposure time, which was more exaggerated in MWIR than LWIR. This increased sensitivity may prove an advantage for feature recognition; however, it may be due to reflections or increased emissions from the UAV battery (or both). LWIR appears to avoid these complications; yet, blade effects generally contribute a higher error in LWIR. The MWIR band's increased sensitivity along with its lower errors imply it may be more likely to produce accurate detection algorithms.

Radiometric trends are also apparent. In almost all cases, absolute intensity increases with respect to increasing aspect angle, likely due to a more visible battery at 45-deg and 90-deg aspect angles. It is well known that a lower number of photons is the most prominent disadvantage in MWIR compared to LWIR, and MWIR absolute intensity values were consistently significantly lower than LWIR values. A notable absolute intensity trend with respect to background type also

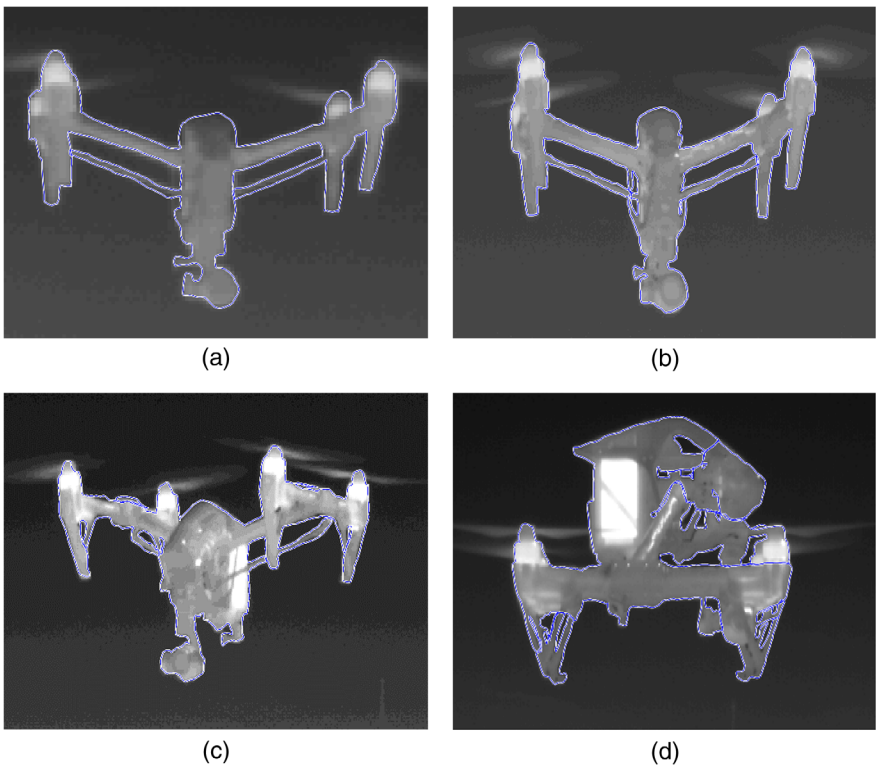

Fig. 7 (a) UAV 2 LWIR signature at 0-deg aspect angle and MWIR signatures at (b) 0-deg, (c) 45-deg, and (d) 90-deg aspect angles in clear sky. Landing gear is in flight mode in the first three images and in the downward position in the last.

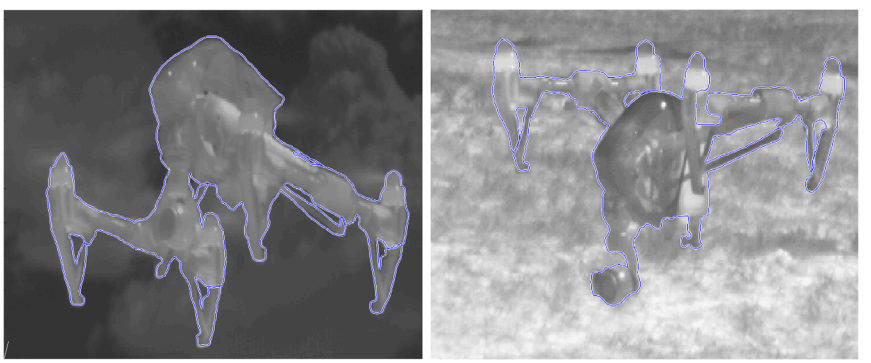

Fig. 8 UAV 2 MWIR signatures at 45-deg aspect angle in cloudy and land backgrounds. Landing gear is in the downward position on the left and flight mode on the right.

appeared, which was specific to each UAV. For the Phantom Pro 4 (UAV 1), land values were higher than those of clear sky, which were higher than those of cloudy sky, for a given aspect. For the Inspire (UAV 2), cloudy sky values were greater than those of land, which were greater than those of clear sky, for a given aspect. The UAV's absolute intensity relationship to its background would help detect a UAV when the model is known or differentiate one UAV from another. Compared to UAV 1, UAV 2 has much higher absolute intensities in MWIR and LWIR with a distinct band characterizing each UAV, encompassing all backgrounds. This is important because specific MWIR and LWIR absolute intensity bands may be used to identify a distinct UAV.

This changes for differential intensity, where patterns become muddled. Generally, differential intensity increases somewhat with respect to aspect angle. However, in three cases, the differential intensities decreased, with 45-deg aspects as the lowest: LWIR UAV 1 clear sky, LWIR UAV 2 land, and MWIR UAV 1 cloudy. Only in one case, MWIR UAV 2 land, did the trend consistently decrease. It is also important to note that zero, low, or negative differential intensities are possible, apparent over land backgrounds. Overall, we find the setting and its level of homogeneity heavily influences differential intensity measurements. This implies that it is necessary to obtain signatures from the field in lieu of artificial, indoor settings to have a more complete and accurate reference.

RSSΔT showed even more variety, where roughly half of the cases increased with aspect and half decreased. Background became the prominent trend here. For UAV 1,

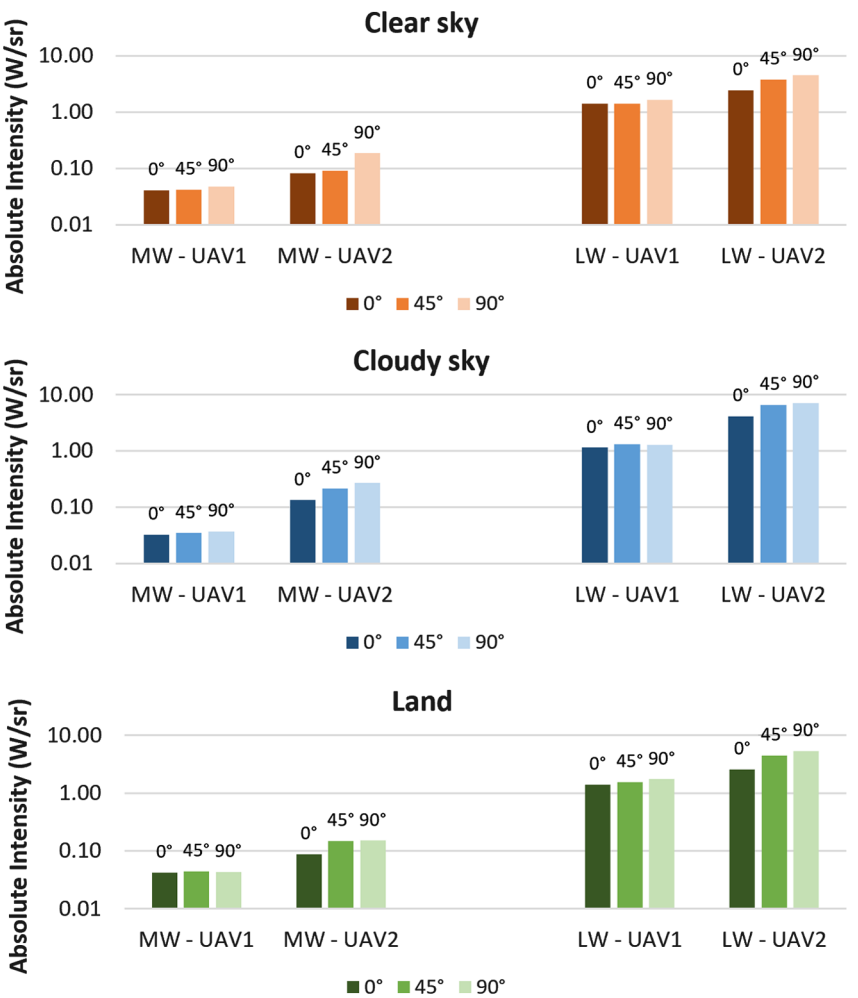

Fig. 9 A graphical summary of absolute intensity trends in each case.

clear sky values were higher than cloudy sky values, which were higher than land values. For UAV 2, cloudy sky values were always higher than clear sky values, which were always higher than land values. These trends identify another characteristic unique to each UAV for use in detection and identification. Also UAV 2 values were consistently higher than UAV 1 values for cloudy and land backgrounds. This trend is particularly useful because these two backgrounds make distinguishing UAVs much harder than it is in clear sky.

To summarize, while absolute intensity increases with respect to aspect angle, possibly a result of battery layout, it varies little. Some land background absolute intensities are slightly higher, but this does not contribute significantly to aspect angle trends because the difference is less than 20%. Possible explanations for the difference are: the target outline may include background intensity, and flux bouncing off the target from the sun or surrounding land creates more reflections. For differential intensity, we find no important trends because the values are highly dependent on background with possible contrast reversal, which confirms the value of imagery and signatures from field collections. Cloudy backgrounds had variations in RSSΔT values, probably due to reflections in the MWIR band and increased emissions in the LWIR band. We reaffirm that LWIR is colder than MWIR for clear sky imagery with the exception of one outlier.

8 Conclusion

We have reported radiometrically calibrated absolute intensity, differential intensity, and RSSΔT for MWIR and LWIR signatures of small, commercial UAVs. This data can be used for targeting, intelligence surveillance, and reconnaissance, as well as discrimination calculations. The values are also useful to decide between MWIR or LWIR trade-offs for a particular application or situation.

It is clear from the analysis of trends that each UAV type has unique absolute intensity patterns in both MWIR and LWIR that can be used as an input for the UAV in algorithms (Fig. 9). LWIR has roughly 30 times more flux than MWIR (as expected), although the LWIR camera has lower resolution than the MWIR camera, presenting a trade-off between competing issues. Differential intensity depends heavily on background, and neither LWIR nor MWIR has a clear advantage with regards to RSSΔT (Fig. 10), though the presented RSSΔT values are good for resolved target discrimination calculations. In conclusion, we show that rather than MWIR or LWIR producing better results than the other, it is the unique absolute intensity and RSSΔT bands of the

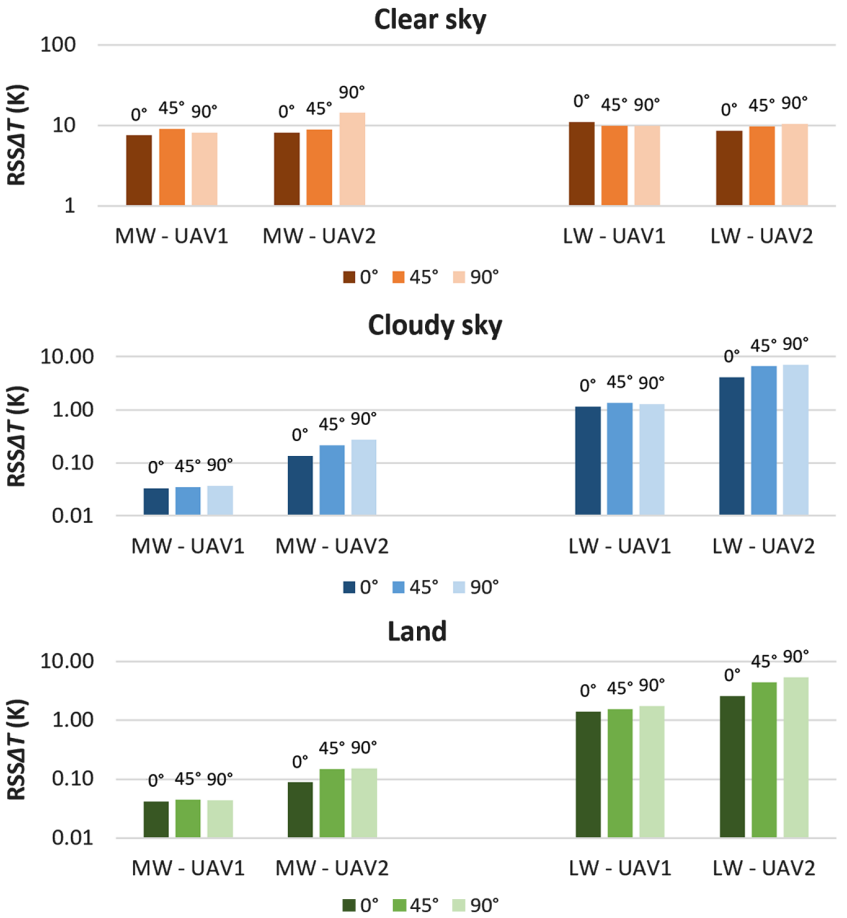

Fig. 10 A graphical summary of RSSΔT trends in each case.

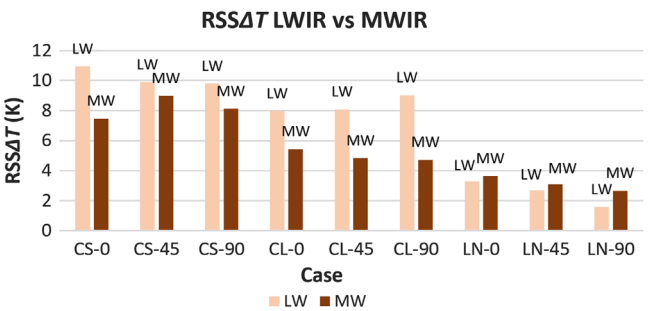

Fig. 11 A comparison of MWIR versus LWIR RSSΔT values for each case.

two MWIR and LWIR ranges together that yield an effective way to detect and identify a particular UAV for IRST. This finding indicates that IR is an appropriate method for UAV detection and tracking.

Considering the results for all three values, especially absolute intensity, LWIR is appropriate to use for overall applications despite the larger errors because it minimizes reflections and there is increased flux in this band, as expected according to the Planck curve. However, we advocate that researchers utilize this analysis to determine for themselves whether LWIR or MWIR is better suited for their specific applications.

9 Future Work

There is little signature data publicly available. This study is one of the first tackling this need, and there remain many avenues for future work in this area. While up close signatures provide more detail, it may also be useful to acquire standard signatures of UAVs at farther distances, especially those close to the transition point from resolved to unresolved. Results also suggest higher temperatures based on UAV operation and/or sun exposure time. Controlling these variables would directly benefit this study and may help clarify the issue.

A future study introducing a highly urban setting and more aspect angles would be beneficial. The Maduro attack occurred after the data collection for this study, confirming that highly developed and populated settings are an important background. A high-quality, 360-deg collection would be especially useful for algorithms geared toward asymmetrical UAVs. IRST would be especially useful in darkness, and many UAV attacks involve payloads. Although the scope of this study only included unladen UAVs during the daytime, signatures at night and involving payloads are also greatly needed. Nighttime signatures may differ significantly, so these tests should be repeated after sundown and before sunrise.

A catalogue of a large variety of UAVs would be valuable, and the potential of identifying an exact UAV model based on its signature characteristics would aid target

Table 6 Difference and error percentage for each blade outline cases.

UAV	IR band	Blade case	Differential intensity difference (%)	RSSΔT difference (%)	Differential intensity error (%)	RSSΔT error (%)
#1 DJI phantom Pro 4	LW	Tgt w/o	1.8973	1.0356	2.3888	2.5548
		Tgt w/B	0.9062	12.3080	−0.4418	−10.2700
		Tot w/o	0.4634	1.4871	N/A	N/A
	MW	Tgt w/o	3.3415	1.3059	−5.3317	−1.0535
		Tgt w/B	5.7538	11.2944	3.6844	−12.7780
		Tot w/o	2.1372	2.3648	N/A	N/A
#2 DJI Inspire	LW	Tgt w/o	4.1954	0.0651	0.2278	0.2581
		Tgt w/B	8.8591	20.3099	5.0183	−18.2802
		Tot w/o	3.9679	0.1927	N/A	N/A
	MW	Tgt w/o	2.2326	0.4333	−1.8206	−2.0186
		Tgt w/B	9.6006	29.8447	5.6941	−27.1489
		Tot w/o	4.0695	1.6060	N/A	N/A

discrimination. This should include fixed wing and rotorcraft designs with a greater number of blades, less common, or asymmetrical shapes, a wider range of UAV materials, and larger and smaller sizes. DJI alone has more rotorcraft designs using six and eight blades, and many other organizations also manufacture UAVs. Toy UAVs down to 3 in. across already exist on the market, and while the drones used in this study were primarily composed of plastic and metal parts, other materials can be used to construct a UAV. Ideally, such a catalogue would have data from all popular, commercially available UAVs. This would aid security and defense organizations in distinguishing between UAVs that are threats and those that are benign.

Acknowledgments

The authors would like to thank those at L3 Technologies for their support in organizing and completing this experiment and those at University of Central Florida, CREOL, The College of Optics and Photonics for supporting the authors. The authors would also like to thank Dr. Eddie Jacobs of the University of Memphis for his assistance and for organizing a space for the field test, Shelby Farms Park in Memphis, Tennessee, for the use of their facilities, and those at 901Drones in Memphis, Tennessee, for the use of their drones and piloting skills. All efforts toward this experiment are greatly appreciated.

References

1. M. Brocchetto et al., "Venezuela makes six arrests in alleged Maduro assassination attempt," *CNN*, https://www.cnn.com/2018/08/05/americas/venezuela-maduro/index.html. (Accessed 6 August 2018).
2. B. Hudson, "First assassination attempt of a president using drones just happened—Here's why it won't be the last," *The Washington Post*, https://www.sciencealert.com/terrorists-now-using-drones-in-assassination-attempts-and-airport-attacks (Accessed 6 August 2018).
3. M. Laurenzis, E. Bacher, and F. Christnacher, "Experimental and rendering-based investigation of laser radar cross sections of small unmanned aerial vehicles," *Opt. Eng.* **56**(12), 124106 (2017).
4. M. Laurenzis et al., "Multi-sensor field trials for detection and tracking of multiple small unmanned aerial vehicles flying at low altitude," *Proc. SPIE* **10200**, 102001A (2017).
5. S. Hengy et al., "Multimodal UAV detection: study of various intrusion scenarios," *Proc. SPIE* **10434**, 104340P (2017).
6. W. Scheller, "Detecting drones using machine learning," Master's Thesis, Iowa State University, p. 16210 (2017).
7. M. Johansson and M. Dalenbring, "Calculation of IR signatures from airborne vehicles," *Proc. SPIE* **6228**, 622813 (2006).
8. R. Nicholas et al., "Infrared search and track performance estimates for detection of commercial unmanned aerial vehicles," *Proc. SPIE* **10625**, 106250Y (2018).
9. M. Gong et al., "IR radiation characteristics and operating range research for a quad-rotor unmanned aircraft vehicle," *Appl. Opt.* **55**, 8757–8762 (2016).
10. P. O'shea et al., "Measuring the infrared intensity of a close-up resolved target with close-up blackbody references," submitted to Redstone Arsenal for release before submission to *Optical Engineering*.
11. R. Driggers, M. Friedman, and J. Nichols, *Introduction to Infrared and Electro-Optical Systems*, Artech House, Boston, Massachusetts (2012).
12. Shelby Farms Park, "Shelby Farms Park & Conservancy," 2019, www.shelbyfarmspark.org (January 2019).
13. DJI, "Phantom 4 Pro," 2019, https://www.dji.com/phantom-4-pro (January 2019).
14. DJI, "Inspire 1," 2019, https://www.dji.com/inspire-1 (January 2019).

Nicolette Fudala received her BS degree in physics and biophysics from Loyola University Chicago in 2017, where she researched neuronal growth and physics education before transitioning to optics and photonic crystal lattice design. She is currently working toward her graduate degree in optics and photonics at the University of Central Florida, CREOL, where she studies IR imaging and optical systems for UAV IRST and related materials.

Jennifer Hewitt holds a BS degree in physics from the University of Maryland, Baltimore County, and is currently studying in the Optics and Photonics Graduate Program at the University of Central Florida. Her research is primarily in the application of hyperspectral cameras in the visible and near-infrared spectral region.

Teresa Pace obtained her doctorate in electrical engineering from The Pennsylvania State University and has 30 years of experience in sensors and systems engineering. She is a director in systems engineering; image and signal processing at L3 Technologies. She is an IEEE fellow, Women in Engineering (WiE) member, past president of Aerospace and Electronic Systems Society (AESS), and former AES editor-in-chief. Her accolades include the Lockheed Martin

Nova Award for outstanding individual technical excellence and HKN outstanding engineer of the year.

Chris Fearing worked at L3 Cincinnati for 7 years on real-time implementations of image processing algorithms. His current focus has been in real-time software systems based in C++ and VHDL for IRST and CUAS projects. His previous projects have included TMSR, image registration, and nonuniformity correction. He has a master's degree in computer engineering, BS degree in computer engineering, and BS degree in electrical engineering from the University of Cincinnati.

Alex Dapore is a senior image processing engineer at L3 Technologies. He received a BSEE and MSEE from the University of Illinois, Urbana–Champaign in 2008 and 2010, respectively. He has worked on research and development projects in many areas of digital image processing. His areas of interest are image restoration, image enhancement, object/threat detection and tracking, multiview computer vision, and the real-time implementation of digital image processing algorithms on GPGPU platforms.

Gene Tener is an electro-optics systems engineer for L3 Space and Sensors in Mason, Ohio. He has over 38 years of electro-optics experience starting with Texas Instruments Defense Systems and Electronics Group in Dallas, Texas, in the early 1980s. In 1987, he moved to Orlando, Florida, and in 2015, he retired as a senior fellow from Lockheed Martin. He was selected twice as the inventor of the year and has over 20 patents.

David Gaudiosi has more than 15 years of experience in the design, development, and application of lasers and optical systems. His expertise includes electro-optic and infrared sensors, ultrashort pulse laser systems, and laser micromachining. Since joining L3, he has been responsible for a variety of optical design and modeling projects, delivering custom sensor solutions and advancing core capabilities. He is a member of SPIE and OSA and has multiple patents issued for ultrashort-pulsed laser micromachining.

Kathleen Richardson is Pegasus Professor of Optics and Materials Science and Engineering and Florida Photonics Center of Excellence (FPCE) and professor at CREOL/College of Optics and Photonics, University of Central Florida. She directs the Glass Processing and Characterization Laboratory (GPCL), where her research team develops novel glass and glass ceramic materials in bulk, film, and fiber form for optical applications, examining the role of structure/property relationships on optical function and performance in the IR spectral region.

Ron Driggers is a professor at the University of Central Florida and has been studying infrared systems for 34 years.

Biographies of the other authors are not available.